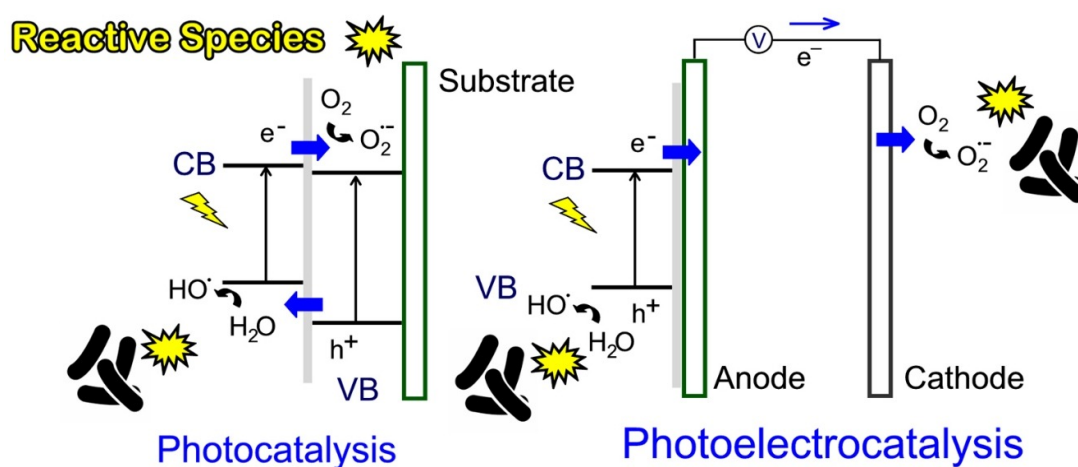


# Critical review on the use of photocatalysis and photoelectrocatalysis to create antimicrobial surfaces

*This manuscript version is provided in accordance with the publisher's policy. Please cite it as follows:*

Laura Valenzuela, Marisol Faraldos, Ana Bahamonde, Roberto Rosal. Critical review on the use of photocatalysis and photoelectrocatalysis to create antimicrobial surfaces. *Current Opinion in Chemical Engineering* 34, 100762, 2021.

<https://doi.org/10.1016/j.coche.2021.100762>



# Critical review on the use of photocatalysis and photoelectrocatalysis to create antimicrobial surfaces

Laura Valenzuela<sup>1</sup>, Marisol Faraldos<sup>2</sup>, Ana Bahamonde<sup>2</sup>, and Roberto Rosal<sup>1,\*</sup>

<sup>1</sup>Department of Chemical Engineering, University of Alcalá, Alcalá de Henares, Madrid E-28871, Spain

<sup>2</sup>Instituto de Catálisis y Petroleoquímica, ICP-CSIC, Marie Curie 2, Madrid E-28049, Spain

## Abstract

Infectious diseases are still a major cause of death worldwide. One way of fighting against infectious agents is to develop intrinsically antimicrobial materials to reduce the risk of pathogen spreading through contact with surfaces. Photoactive coatings offer the possibility to produce long-lasting antimicrobial surfaces that destroy microorganisms or biofilm matrices due to the production of highly reactive substances when exposed to ultraviolet light or solar radiation. This review reports a selection of recent works using materials deposited on different substrates to act as photocatalytic or photoelectrocatalytic coatings. Bandgap engineering with the introduction of dopants, or the creation of different junctions allow gaining stability, limit the rate of electron-hole recombination, and can produce materials photoactive under the visible wavelengths of the solar spectrum.

## Introduction

Despite the huge advances in the fight against pathogens, communicable diseases still represent over 10 million deaths annually. Infections caused by bacteria, virus, fungi, and parasites predominantly affect people living in low-income countries, but epidemic waves like HIV/AIDS and the current Covid-19 show that nobody is free to be severely affected by infectious diseases. Antimicrobial resistance has emerged as one of the major public health concerns declared by the World Health Organization one of the top 10 global public health threats to humanity. Besides, chronic diseases, aggressive medical treatments, population ageing, and co-infections like in HIV+ patients, are increasing the occurrence of opportunistic infections, which find an easier way in immunocompromised persons.

Pathogens spread in different ways, in many cases directly for person to person, but there is evidence that important pathogens persist for extended periods on surfaces at concentrations high enough to be infective [1]. Conventional disinfection traditionally involves the use of chemicals, ultraviolet radiation, or heat to reduce the load of pathogens until they became below infective doses. However, many microorganisms developed an evolutionary strategy to fight against hostile environments and form biofilms. Biofilms are highly structured communities of mi-

croorganisms that create their own environment embedded in a self-produced extracellular matrix, are sometimes multispecies and can be considered only one step below pluricellular organisms. Biofilms are responsible for many infections and are of particular concern because once formed they are very resistant to conventional disinfection processes [2].

A strategy to fight against infections consists of developing intrinsically clean surfaces. The goal is to reduce infection risks by limiting the exposure to infectious agents, which means reducing the number of pathogens that can be transferred to a new host. The number of active pathogens below which the risk of transmission is negligible, depends on the type of infectious agent and can be estimated using quantitative microbial risk assessment models [3]. Antimicrobial surfaces can be broadly classified as passive or active. Passive surfaces reduce the initial adhesion of microbes, while active surfaces kill them upon contact. Passive or anti-biofouling surfaces frequently use bioinspired approaches based on superwettability, superhydrophobicity, superoleophobicity and omniphobicity to resist microbial colonization [4]. Active antimicrobial surfaces include metals, like silver or copper, which are capable of impairing pathogenic cells, but have the drawback of a limited durability and pose environmental or health concerns. An alternative approach to produce active self-cleaning surfaces is to use photocatalytic coatings. Photocatalytic coatings can produce long-lasting antimicrobial surfaces that destroy microorganisms or biofilm matrices due to the generation of highly reactive radicals when exposed to ultraviolet light or solar radiation [5].

\* Corresponding author: roberto.rosal@uah.es

Available online: November 11, 2021

## The antimicrobial action of photocatalysts

Semiconductors have been widely used as photocatalysts for pollutant removal for both air pollution control and water treatment. Upon irradiation of the adequate wavelength, an electron is excited from the valence band (VB) to the conduction band (CB) of the semiconductor creating an electron-hole ( $e^-$ - $h^+$ ) pair. The excited electron can reduce an acceptor and the hole may oxidize an electron donor. The participation of oxygen and water may produce oxidizing species like superoxide ( $O_2^{\cdot-}$ ) and hydroxyl ( $HO\cdot$ ) radicals upon interaction with electrons (oxygen) and holes (water molecules), respectively. Both radicals exhibit strong oxidation capacity and participate in a series of reactions that involve other oxidants, globally referred to as reactive oxygen species (ROS). ROS are capable to inactivate microorganisms because they can interfere with important metabolic and signalling microbial functions and disrupt cell envelopes, eventually compromising cell viability.

Many semiconductors have been tested as photocatalysts. The main aspect governing their activity is the position of band edges and the energy required to transfer one electron from the VB to the CB, or band gap. Many investigations have been performed to enhance the stability of photocatalysts, to reduce the rate of electron-hole recombination, and to obtain materials capable of harvesting the visible component of the solar energy spectrum [5, 6]. The use of dopants is a well-known strategy to tune properties like semiconductor type and to increase the range of absorbed wavelengths. N-doped  $TiO_2$  has a reduced band gap due to the formation of intragap states close to the VB. Besides, doping can modify band positions, which determine the redox capacity of electrons and holes. For example, boron doped in  $TiO_2$  was shown to move the position of VB (+0.4 eV) and CB (+0.6 eV) [7]. In another example, Cu-doped  $TiO_2$  nanocrystals possess intragap states  $\sigma^*(1)$ ,  $\sigma^*(2)$  and  $\pi^*$  due to the interaction of 3d orbitals from Cu with O  $p\pi$  and  $p\sigma$  orbitals. The result is that Cu- $TiO_2$  absorbs at 2.0–2.2 eV ( $\sim 1$  eV less than  $TiO_2$ ) corresponding to the transition from VB to  $\sigma^*(1)$  and from  $\pi^*$  to  $\sigma^*(2)$  as shown in Figure 1a [8].

The creation of heterojunctions is another strategy to avoid  $e^-$ - $h^+$  recombination. The behaviour of a heterojunction depends on the alignment of the bands at the interface. The most useful in photocatalysis is the staggered gap, known as Type II [9]. An example is shown in Figure 1b, that corresponds to a heterojunction between p-type CuO and n-type  $BiVO_4$ . The photogenerated electrons move from the CB of p-type CuO (band gap 1.70 eV) to the CB of

$BiVO_4$ . Conversely the holes in the VB of  $BiVO_4$  are transferred to that of CuO, reducing electron-hole recombination rate [10]. Although not shown in the figure, the band bending generated at the interface creates an internal electric field that drives photogenerated electrons to the CB of the n-type semiconductor ( $BiVO_4$ ) and holes to the VB of the p-type semiconductor (CuO), inducing the movement of electrons and holes in opposite directions [11].

Another type of junction is that formed between metals and semiconductors. Two different types exist: Schottky junction and Ohmic contact, which differ in the direction of the photogenerated electrons, which move from semiconductors to metals in Schottky junctions and from metals to semiconductors in Ohmic contacts [12]. If band bending forces the electric field to point to the semiconductor, the photogenerated electrons tend to accumulate in the metal avoiding electron-hole recombination. There is also the possibility of using plasmonic electrons to produce reactive radicals with the benefit of using low energy radiation, including infrared wavelengths. The surface plasmon resonance (SPR) effect is illustrated in Figure 1c, which corresponds to Au/ $Bi_2WO_6$  irradiated with near infrared (NIR). In this case, the electrons photogenerated in Au are transferred to  $Bi_2WO_6$  across the Schottky barrier at the Au/ $Bi_2WO_6$  interface where they can reduce oxygen to produce ROS [13, 14].

## Photocatalytic coatings

Many methodologies have been developed to immobilize photocatalysts onto solid supports. The physical deposition of finely dispersed materials can be achieved by spin-coating, dip-coating, or spray-coating. The same overall concept is used by thermal spray and physical vapour deposition like sputter deposition or magnetron sputtering. In some cases, a precursor reacts or decomposes on the surface to yield the photocatalytic coating like in chemical vapour deposition or atomic layer deposition techniques. Some techniques require electric fields like anodic oxidation, in which an oxide film forms directly on an anodic surface, electrophoretic deposition or the electrohydrodynamic technique known as electrospray.

$TiO_2$  is still the most used photocatalyst to produce antimicrobial surfaces by means of different techniques like impregnation, electrospray, and magnetron sputtering [15, 16, 17, 18]. The relatively large bandgap of  $TiO_2$  (3.2 eV for anatase and 3.0 for rutile) explains the efforts made to increase its capacity to convert lower energy photons into electron-hole pairs. Cu-decorated  $TiO_2$  showed enhanced bacte-

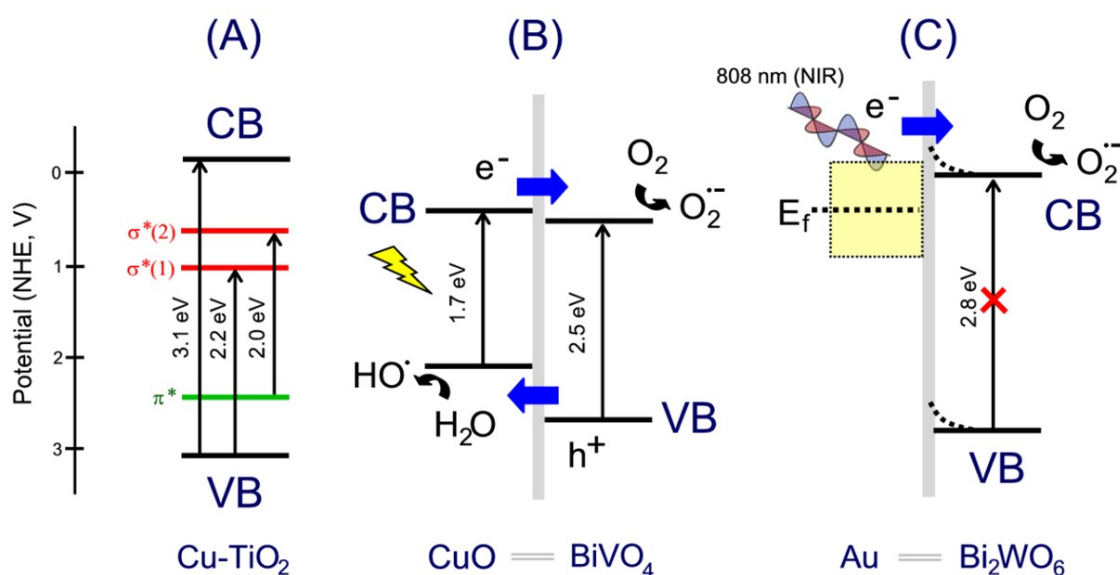


**Figure 1:** (a) Band structure of Cu-doped  $\text{TiO}_2$  [8]; (b) type II heterojunction formed with  $\text{CuO}$  and  $\text{BiVO}_4$  [10, 11]; (c) Schottky barrier formed between  $\text{Au}$  and  $\text{Bi}_2\text{WO}_6$  [13, 14].

rial inactivation due to a better charge separation obtained from Cu intragap states [19]. The doping of  $\text{TiO}_2$  with non-metals is another usual strategy to decrease band gap. In the case of F-doped  $\text{TiO}_2$ , the reduction is due to the induction of surface  $\text{Ti}^{3+}$  defects below the CB [20].

$\text{ZnO}$  is an n-type semiconductor with bandgap of 3.3 eV frequently reported for photocatalytic applications, but  $\text{ZnO}$  suffers corrosion and photocorrosion. This phenomenon, that limits stability and durability, enhances the antimicrobial capacity of  $\text{ZnO}$ -based coatings as  $\text{Zn}^{2+}$  induces intracellular ROS overproduction [21, 22]. The work function of reduced graphene oxide (rGO) changes in the 4.5–5.5 eV depending on its oxygen content [23]. This value is close to the work function of  $\text{ZnO}$  and therefore, a suitable Schottky or ohmic junction can be formed in which the electrons move easily from the CB of  $\text{ZnO}$  to rGO, reducing the high recombination rate of pure  $\text{ZnO}$  [24].  $\text{Ag}/\text{ZnO}$  heterojunction demonstrated good photocatalytic activity due to SPR effect. In addition,  $\text{Ag}$  can be inserted into the  $\text{ZnO}$  lattice to create a type II heterojunction between  $\text{Ag}_x\text{Zn}_{1-x}\text{O}$  and  $\text{ZnO}$  [25].

Bismuth oxide ( $\text{Bi}_{44}\text{O}_{56}$ ,  $\sim\text{Bi}_2\text{O}_3$ , band gap 2.4 eV) and bismuth tungstate ( $\text{Bi}_{27}\text{W}_{11}\text{O}_{62}$ ,  $\sim\text{Bi}_2\text{WO}_6$ , band gap 2.6 eV) were used to produce antimicrobial coatings active under visible light irradiation [26].  $\text{Bi}_2\text{WO}_6$  heterostructures with noble metals may benefit from the synergy between surface plasmon resonance (SPR) and the formation of Schottky junctions [12]. Based on this principle,  $\text{Au}$  nanorod decorating bismuth tungstate ( $\text{Bi}_2\text{WO}_6$ ) nanosheets, demon-

strated antimicrobial activity under near infrared (NIR) irradiation [13].  $\text{WO}_3$  is an n-type semiconductor with narrow bandgap (monoclinic: 2.4–2.8 eV);  $\text{ZrO}_2$  is wide band gap (5.2 eV) n-type semiconductor only excitable with high energy radiation but might improve catalyst stability.  $\text{Ru}/\text{WO}_3\text{-ZrO}_2$  photocatalyst was an active antimicrobial material, probably due to the formation of a Schottky junction at the  $\text{Ru}/\text{WO}_3$  or  $\text{RuO}_2/\text{WO}_3$  interface, which would promote the transfer of photogenerated electrons from  $\text{WO}_3$  CBs to  $\text{Ru}$  or  $\text{RuO}_2$  [27, 28].  $\text{CuO}/\text{BiVO}_4$  nanocomposite photocatalyst activity was attributed to the charge transfer from n-type  $\text{BiVO}_4$  to p-type  $\text{CuO}$  nanoparticles due to the transfer of electrons and holes as explained above [29].  $\text{CuO}/\text{BiVO}_4$  was used to prepare antimicrobial cotton fabrics active under visible light [10]. Another example of a type II heterojunction is provided by  $\text{ZnO}$  and  $\text{TiO}_2$ , which are particularly suited to that purpose because both CB and VB edges of  $\text{ZnO}$  are higher than their counterparts in  $\text{TiO}_2$  [30].

## Photoelectrocatalysis

Photoelectrocatalysis (PEC) reduces charge carrier recombination by immobilizing the photocatalyst on an electrically conducting support to which a bias potential is applied while irradiating, thus continuously extracting photoexcited electrons. As a result, electrons are transferred from the CB to the counter electrode (cathode) through the external circuit while holes accumulate on the catalyst surface (photoanode). The separation of oxidation and reduction reac-

tions increases quantum yield and faradaic efficiency counterbalancing the mass transfer limitations due to the immobilization of the photocatalyst [31•, 32].

PEC performance is influenced by several parameters, apart from the photocatalyst itself. The main ones are the cathode material, the bias potential, the type of electrolyte, the photoreactor configuration, and the irradiation wavelength. Table 1 shows a selection of recent works on PEC disinfection including details on photoanode fabrication method, cell configuration, and disinfection performance. Although Pt remains the most widely used cathode material because of its good chemical resistance and low reduction overpotential [33, 34, 35, 36•, 37, 38, 39, 40••], carbon-based electrodes have been shown to enhance disinfection rate due to their selectivity towards the reduction of dissolved molecular oxygen to hydrogen peroxide ( $H_2O_2$ ).  $H_2O_2$  can penetrate cell membrane and react with intracellular iron producing internal  $HO\cdot$  or undergone one electron reduction yielding  $HO\cdot$  at the cathode [36•, 41••, 42].

The optimal applied bias potential for a photocatalytic electrode in PEC (i.e. potential at which the maximum photocurrent and thus maximum separation of photogenerated electron-hole pairs are obtained) depends on reactor configuration and electrolyte conductivity. A value of 1.0 V is frequently reported, which is lower than that required in electrocatalytic processes [31•, 32, 34, 36•, 37, 40••, 41••]. It has been shown that disinfection performance does not improve when increasing the applied bias potential upon that required to separate charge carriers [31•]. Moreover, excessive current can lead to unfavourable reactions such as the evolution of  $H_2$  and  $O_2$  or the reduction of  $H_2O_2$  to  $H_2O$  [43].

Increased electrolyte conductivity leads to a higher current density but also to a lower electromigration of bacteria towards the photoanode [49]. Besides, the specific ion composition influences PEC performance by altering the type of oxidant species generated. Although  $HO\cdot$  is the main radical involved in microbial inactivation, active chlorine species and sulphate radicals can also be produced in the presence of chloride and sulphate [40••, 50]. Juodkazytė et al. showed that the formation of hydroxyl radicals and chlorine species can take place simultaneously in  $WO_3$  due to the energy of VB photogenerated holes and the proximity of the standard potentials of both reactions [35]. However, a high ionic strength leads to an antagonistic effect because of ROS scavenging by active chlorine species [44]. Carbonate is another well-known radical scavenger that decreases photocurrent density and PEC efficiency [37].

Regarding photoreactor configuration (Figure 2), most PEC disinfection treatments use undivided cells,

stirred either mechanically, or by bubbling air or oxygen [49]. Conventional two or three-electrode stirred tank reactors are widely used [33, 36•, 40••, 48]. However, other configurations like cylinder reactors gained attention due to a better use of light, including their compatibility with Compound Parabolic Collectors (CPC) [32, 41••, 43]. Thin electrochemical cells, such as sandwich or microchannel photoreactors have also been proposed to increase surface to volume ratio and to overcome mass transfer limitations [34, 36••]. Finally, three-dimensional electrode reactors have been reported for PEC bacterial inactivation, in which anode and cathode are conventional electrodes, the supported photocatalyst (3D) acting as bipolar electrode [44].

The photoanode includes the photocatalyst deposited on a conductive support. The support can be metallic [31•, 33, 34, 36•, 37, 39, 41••, 43, 46], carbonaceous [44, 48], ITO, or tin-oxide-based (fluorine-doped tin oxide, FTO or indium tin oxide, ITO) [32, 35, 38, 40••, 45, 47]. The most widely used photoactive material for PEC disinfection is  $TiO_2$  in different forms. Vertically aligned  $TiO_2$  nanotube arrays (TNTs) stand out owing to their high surface area, excellent stability, and superior photoelectron transport capability [31•, 34, 36•, 41••, 43, 46]. PEC using TNTs demonstrated capacity to inactivate antibiotic-resistant bacteria (ARB) and its associated antibiotic resistance genes (ARG), which can persist after host bacteria inactivation [34]. The cathodic polarization of TNTs leads to an enrichment of  $Ti^{3+}$  species on their surface, with increased capacitance and visible light absorption due to the formation of mid-gap states [31•]. Ag-decorated  $TiO_2$  films exhibited a faster bacterial inactivation than bare  $TiO_2$  ascribed to the transfer of electrons from the VB of  $TiO_2$  to Ag nanoparticles, thereby suppressing charge carrier recombination and promoting  $HO\cdot$  production on the photoanode [45].  $Cu_2O/TiO_2$  p-n heterojunction deposited onto Cu mesh exhibited strong durability, improved visible light absorption and a better separation of photogenerated electron-hole pairs, thus promoting PEC bacterial disinfection [33].  $MoS_2$  nanosheets were partially oxidated to form  $MoS_2/MoO_x$  heterojunction can be photoexcited by visible light with improved PEC disinfection performance attributed to the separation of photogenerated holes (in  $MoS_2$ ) and electrons (in  $MoO_x$ ) [39].  $BiVO_4$  and  $WO_3$  have also been tested as catalysts for PEC disinfection based on their capacity to harvest visible light, excellent resistance to photocorrosion, adequate band structure to produce strong oxidizing holes, low-cost, and non-toxicity [35, 37, 40••].  $ZnWO_4$  has been used in PEC for the deactivation of marine microorganisms owing to its high oxygen evo-

Table 1. Selection of recent works on photoelectrocatalytic (PEC) disinfection.

Photoanode	Fabrication method and photocatalyst structure	Photoelectrochemical cell configuration	Disinfection performance	Reference
TNTs on Ti foil (9.5 cm <sup>2</sup> ).	Electrochemical anodization and cathodic self-doping; multi-porous layer structure with diameter ~100 nm and length ~16 μm.	Cathode: Pt coil. Applied potential: 1.0 V vs. Ag/AgCl. Electrolyte: 0.1M Na <sub>2</sub> SO <sub>4</sub> (2.2 mS cm <sup>-1</sup> ) and tap water (0.21 mS cm <sup>-1</sup> ). Reactor: conventional three-electrode system (40 mL), average electrode distance of 1 cm. Irradiation: Six 4 W black light UVA lamps, peak wavelength at 352 nm, 2.5 mW cm <sup>-2</sup> .	Photoelectrocatalysis: 3-log inactivation of <i>E. coli</i> and MS2 coliphage in 10 min. Electrocatalysis and photolysis: unclear results.	[31]
TiO <sub>2</sub> on ITO (5 × 5 cm or scaled-up cylindrical tubes with 15 cm long, 3 cm inner-tube diameter and 5 cm external-tube diameter).	Dip-coating; thickness layer 0.88 ± 0.12 μm.	Cathode: Nickel mesh. Applied potential: 1.0 V. Electrolyte: 0.1 M Na <sub>2</sub> SO <sub>4</sub> (16 mS cm <sup>-1</sup> ) or simulated wastewater treatment plant effluents (SWTPE, 40 μS cm <sup>-1</sup> ). Reactor: two-electrode system (0.4 L, stirred, 1 cm between electrodes or scaled-up cylindrical two-electrode system (1 L), 15 cm long, 3 cm inner-tube diameter and 5 cm external-tube diameter operating in a closed recirculating circuit; counter and working electrodes separated 0.5 cm. Irradiation: 6 W black light lamp, maximum emission peak at 365 nm, 0.70 W m <sup>-2</sup> or 0.47 W m <sup>-2</sup> .	Photoelectrocatalysis: increased bacterial inactivation kinetic constants in comparison to photocatalysis from 1.45 up to 2.18 × 10 <sup>4</sup> CFU L <sup>-1</sup> min <sup>-1</sup> in 0.1 M Na <sub>2</sub> SO <sub>4</sub> and from 1.73 up to 2.23 × 10 <sup>4</sup> CFU L <sup>-1</sup> min <sup>-1</sup> in SWTPE for <i>E. coli</i> . Scaled-up photoelectrodes for the annular reactor showed less bacterial inactivation because of back-side illumination.	[32]
Cu <sub>2</sub> O/TiO <sub>2</sub> on Cu mesh (2.0 × 2.0 cm).	Supercritical solvothermal method; microspheres with a diameter of ~2.0 μm.	Cathode: Pt foil (2.0 × 2.0 cm). Applied potential: 0.2 V vs. Ag/AgCl. Electrolyte: Phosphate-buffered saline (PBS). Reactor: conventional three-electrode system (30 mL, stirred). Irradiation: visible light irradiation, 300 W, Xe lamp with 420 nm cut-off filter.	Photoelectrocatalysis: total inactivation of <i>Acinetobacter baumannii</i> in 30 min; higher inactivation rate compared with photocatalysis. Photocatalysis: complete inactivation of <i>A. baumannii</i> in 30 min; Electrocatalysis and photolysis: no effect.	[33]

**Table 1 (Cont.).** Selection of recent works on photoelectrocatalytic (PEC) disinfection.

Photoanode	Fabrication method and photocatalyst structure	Photoelectrochemical cell configuration	Disinfection performance	Reference
Titanium dioxide nanotubes.	Electrochemical anodization; nanotubes with inner diameter of ~80 nm and 8 $\mu\text{m}$ length.	Cathode: Pt foil. Applied potential: 1.0 V vs. Ag/AgCl. Electrolyte: 0.2 M NaClO <sub>4</sub> . Reactor: flow-through thin-layer (0.20 mm) three-electrode photoelectrochemical reactor (300 $\mu\text{L}$ ). Irradiation: LED lamp, maximum wavelength at 365 nm, 28 mW cm <sup>-2</sup> .	Photoelectrocatalysis: inactivation of antibiotic-resistant <i>E. coli</i> S1-23 and removal of its associated antibiotic resistance genes <i>blaTEM-1</i> and <i>aac(3)-II</i> in 10 and 16 h, respectively. Photocatalysis and electrocatalysis: no effect.	[34]
WO <sub>3</sub> on FTO (1 $\times$ 2.5 cm).	Sol-gel method with polyethylene glycol (PEG) as an additive and drop casting technique; 400 nm-sized plates, mixture nanoplates and nanosheets.	Cathode: Pt plate (1 $\times$ 1 cm). Applied potential: 1.6 V vs. Ag/AgCl. Electrolyte: 0.5 M NaCl. Reactor: two-compartment quartz cell, 0.22 $\mu\text{m}$ pore size filter. Irradiation: Xe lamp with 6000 K spectrum, ~100 mW cm <sup>-2</sup> .	Photoelectrocatalysis: 5.72-log reduction for <i>Bacillus</i> sp. and complete disinfection for <i>E. coli</i> , attributed to reactive chlorine species. Electrocatalysis and photolysis: No effect for <i>Bacillus</i> sp. and 1.4-log reduction for <i>E. coli</i> .	[35]
Self-assembled TiO <sub>2</sub> nanotubes on Ti mesh electrodes 75 $\times$ 95 mm <sup>2</sup> .	Electrochemical anodization; nanotubes with average outer diameter of 95.2 nm, inner diameter 73.6 nm, tube wall thickness of 21.6 nm and 1.05 $\mu\text{m}$ average length.	Cathode: Pt and carbon felt; Applied potential: 1.0 V. Electrolyte: surface water (697 $\mu\text{S cm}^{-1}$ ). Reactor: anode-anode-cathode configuration (190 mL) with an air-blower (0.36 mL min <sup>-1</sup> ). Irradiation: two 9 W UVA black light lamps, 370 nm-peak wavelength, irradiance 50 W m <sup>-2</sup> .	Photoelectrocatalysis: <i>E. coli</i> , 2-log for Pt and 2.7-log reduction for carbon felt in 2 h. 4.5-log reduction in 90 min for the degradation of microcontaminants and inactivation of <i>E. coli</i> . Photocatalysis: <i>E. coli</i> , 0.8-log reduction.	[36]
W/WO <sub>3</sub> .	Electrochemical anodization; outer diameter ~100 nm and lengths of the order of tens of microns.	Cathode: Pt gauze. Applied potential: 1.0 V vs. Ag/AgCl. Electrolyte: haemodialysis dialysate. Reactor: conventional three-electrode system (250 mL), stirred by air supply, cooling system (19 °C). Irradiation: UV-vis by Mercury vapor lamp 125 W and visible irradiation using borosilicate filter.	Photoelectrocatalysis: Inactivation of <i>C. parapsilosis</i> within 1 min and ~40% degradation of the by-products generated due to cell lysis in 120 min. Photocatalysis and photolysis: 5 and 10 times slower than photoelectrocatalysis.	[37]

Table 1 (Cont.). Selection of recent works on photoelectrocatalytic (PEC) disinfection.

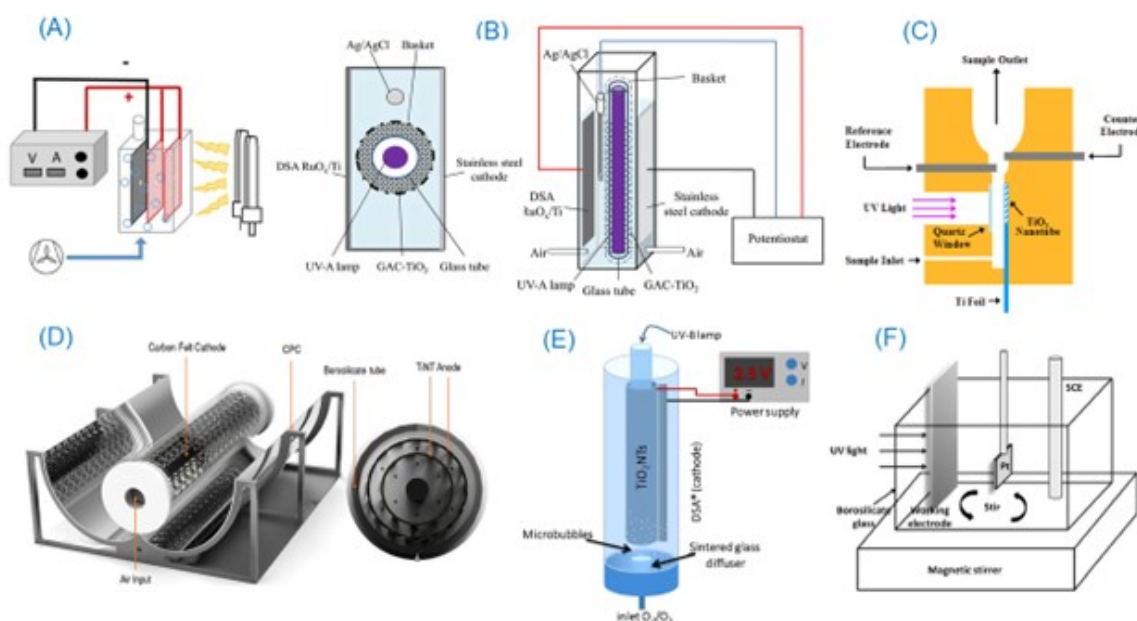
Photoanode	Fabrication method and photocatalyst structure	Photoelectrochemical cell configuration	Disinfection performance	Reference
GO/ZnWO <sub>4</sub> on ITO (60 × 20 mm).	Dip-coating with Nafion; nanorod structure.	Cathode: Pt. Applied potential: 2.0 V vs. SCE. Electrolyte: seawater. Reactor: conventional three-electrode system (100 mL). Irradiation: 12 W, 254 nm wavelength.	Photoelectrocatalysis: <i>Chlorella</i> (no species given) completely removed in 8 min. Electrocatalysis: total removal in 10 min. Photocatalysis: total removal in 20 min.	[38]
Ti/MoS <sub>2</sub> /MoO <sub>x</sub> on Ti foil 7 × 12 cm or 7 × 6 cm.	Dip-coating with Nafion; nanorod structure	Cathode: Pt foil or Ti film (12 × 7 cm). Applied potential: 0.5 V vs. Ag/AgCl or 1.0-1.5 V vs. Ag/AgCl. Electrolyte: 0.1M NaCl. Reactor: conventional three-electrode system (100 mL) or scaled-up two-electrode reactor (3 L, 1-5 cm between electrodes). Irradiation: visible light (300 W Xe lamp, 420 nm filter, 95.5 mW cm <sup>-2</sup> ) or 100 W LED lamp irradiation (25-74 mW cm <sup>-2</sup> ).	Photoelectrocatalysis: complete inactivation of 10 <sup>6</sup> CFU mL <sup>-1</sup> <i>E. coli</i> in 2 h. Scale-up experiments: inactivation ranging from 0.5-log to 4-log for 1.0 to 1.5 V in 6 hours. Electrocatalysis and photolysis: 0.5-log reduction of <i>E. coli</i> .	[39]
BiVO <sub>4</sub> on ITO (40 × 20 × 2.0 mm).	Electrodeposition-annealing; dense BiVO <sub>4</sub> film with particle units, ~80 nm thickness.	Cathode: Pt foil. Applied potential: 1.0 V vs. Ag/AgCl. Electrolyte: Sewage with 1.5 mM Na <sub>2</sub> SO <sub>3</sub> . Reactor: conventional three-electrode system (100 mL), distance between the cathode and the photoanode ~3 cm. Irradiation: visible light, 300 W Xe lamp with a 420 nm UV cut-off filter.	Photoelectrocatalysis: simultaneous degradation of pharmaceuticals and personal care products, hydrogen evolution and <i>E. coli</i> disinfection. <i>E. coli</i> reduction > 4-log in 5 cycles.	[40]
Aligned titania nanotubes on cylindrical Ti mesh.	Electrochemical anodization; nanotubes with length of 2.37–2.52 μm and average diameter of 92 nm.	Cathode: carbon felt. Applied potential: 1.0 V. Electrolyte: rainwater (70 μS cm <sup>-1</sup> ). Reactor: concentric tubular configuration (300 mL), CPC (concentration factor of 1), two anodes with different diameter and cathode at the centre. Irradiation: real sun during winter in South Africa (max: 13 W m <sup>-2</sup> ).	Photoelectrocatalysis: 5.5- and 5.8-log reduction for <i>E. coli</i> and <i>P. aeruginosa</i> ; 2.4- and 3.0-log reduction in <i>E. coli</i> and <i>P. aeruginosa</i> gene copies. Photolysis: 3.1- and 2.7-log reduction for <i>E. coli</i> and <i>P. aeruginosa</i> ; gene copies: 0.45- and 0.91-log reduction for <i>E. coli</i> and <i>P. aeruginosa</i> ; 4 hours in all cases.	[41]

Table 1 (Cont.). Selection of recent works on photoelectrocatalytic (PEC) disinfection.

Photoanode	Fabrication method and photocatalyst structure	Photoelectrochemical cell configuration	Disinfection performance	Reference
Cylindrical TiO <sub>2</sub> nanotubes electrode (6.5 cm diameter and 31.5 cm length, 1000 cm <sup>2</sup> internal geometric area).	Electrochemical anodization; nanotubes with average diameter 68.2 ± 5.1 nm, tube wall 14.6 ± 1.5 nm, length 2.42 μm.	Cathode: DSA® sheet (110 cm <sup>2</sup> ). Applied potential: 2.0 V. Electrolyte: simulated and real contaminated swimming pool water. Reactor: annular bubble reactor (7.6 cm diameter, 1 L), sintered glass bubbler for injecting O <sub>2</sub> /O <sub>3</sub> . Irradiation: UV-B narrowband 36 W lamp.	Photoelectrocatalysis + ozonation: simultaneous degradation of sunscreen, benzophenone-3, urea and fungi ( <i>Candida parapsilosis</i> , completely inactivated after 45 min.	[43]
TiO <sub>2</sub> on activated carbon, GAC-TiO <sub>2</sub> (bipolar electrode, 1.5 mm in length × 0.5 mm in diameter) RuO <sub>x</sub> /Ti anode (10×10 cm).	High temperature impregnation method; non-homogeneous distribution of on the external surface of GAC.	Cathode: stainless steel sheet. Current density: 0.10 mA cm <sup>-2</sup> . Electrolyte: simulated fish farm seawater. Reactor: 3D reactor (6.5×11×22 cm); air flow of 0.1 L s <sup>-1</sup> . Irradiation: 6 W UV-A light, 365 nm, 3.60·10 <sup>-6</sup> E s <sup>-1</sup>	Photocatalysis: <i>E. coli</i> removal > 99% (>2-log) in 120 min. Electro-catalysis: inactivation >99% of <i>E. coli</i> in 90 min. Photoelectrocatalysis: no further improvement.	[44]
Ag-decorated TiO <sub>2</sub> (4 wt% Ag) on ITO (3 cm <sup>2</sup> )	Electrochemical deposition (TiO <sub>2</sub> ) and impregnation (Ag); cuboid-shaped Ag and non-spherical TiO <sub>2</sub> particles with a size of ~45 nm and 100 nm, respectively.	Cathode: stainless steel spiral. Applied potential: 1.7 V vs. Ag/AgCl. Electrolyte: 25 mM Na <sub>2</sub> SO <sub>4</sub> . Reactor: conventional three-electrode system (100 mL), cooling system 25 °C). Irradiation: 125 W UVA light bulb ( $\lambda_{max}$ 360 nm), placed in parallel at a distance of 6 cm.	Photoelectrocatalysis: total inactivation of <i>Pseudomonas aeruginosa</i> and <i>Bacillus atrophaeus</i> in 5 and 15 min, respectively. Photocatalysis: 40 min for the complete inactivation of <i>Pseudomonas aeruginosa</i> .	[45]
TNTs-Ag/SnO <sub>2</sub> -Sb) on Ti plate 30 × 30 × 3 mm.	Electrochemical anodization (TNTs), sol-gel dip-coating (TNTs/SnO <sub>2</sub> -Sb) and electrodeposition (Ag); TNTs with a diameter of 80-150 nm, SnO <sub>2</sub> -Sb on top of TNTs with similar diameter as TNTs, small Ag powders forming a thin coating.	Cathode: carbon/polytetrafluoroethylene (PTFE). Current density: 4 mA cm <sup>-2</sup> . Electrolyte: 100 mM Na <sub>2</sub> SO <sub>4</sub> . Reactor: conventional three-electrode system (100 mL), cooling system (20 ). Irradiation: Simulated sunlight 250 W Xe lamp.	Photoelectrocatalysis: simultaneous removal of 17 $\alpha$ -ethinylestradiol and <i>E. coli</i> . 5-log removal of <i>E. coli</i> in 1 h. Photocatalysis, electrocatalysis and photolysis: 4-log removal of <i>E. coli</i> in 1 h. Photocatalysis outperformed electrocatalysis.	[46]

**Table 1 (Cont.).** Selection of recent works on photoelectrocatalytic (PEC) disinfection.

ZnWO <sub>4</sub> /ITO (3 cm <sup>2</sup> ).	Hydrothermal method and coating with PTFE as film former agent; nano-sized bars with an average length of 200 nm and width of 50 nm.	Cathode: Ti (30 × 10 mm). Applied potential: 3.0 V vs. SCE. Electrolyte: Seawater. Reactor: conventional three-electrode system (150 mL). Irradiation: UV (12 W, 254 nm).	Photoelectrocatalysis: [47] Chlorella completely deactivated in 10 min. Photocatalysis: deactivation 3 times slower.
TiO <sub>2</sub> composites with 1.5-2.0 wt% Ce and 2 wt% GO.	Electrosprayed onto 2.5 × 2.5 cm graphite paper; thickness of the photocatalytic layer 1.0-1.5 μm; mean roughness 45.7 nm.	Cathode: graphite paper. Applied potential: 0.6 V vs. Ag/AgCl. Electrolyte: 1/10 NB (nutrient broth), electrical conductivity: 1200 μS cm <sup>-1</sup> . Reactor: conventional three-electrode system (20 mL). Irradiation: 365 nm LED light, irradiance 3.0 kW-h m <sup>-2</sup> day <sup>-1</sup> .	Photoelectrocatalysis: [48] 3-log inactivation of <i>S. aureus</i> for Ce-TiO <sub>2</sub> /GO anodes after 24 min. The anodes were pre-exposed for 20 h to growing cultures of <i>S. aureus</i> . PEC outperformed photocatalysis and electrocatalysis.

**Figure 2:** Different configurations for PEC reactors. (a) Sandwich-type [36●]; (b) 3D electrode reactor [44]; (c) Flow-through thin-layer [34]; (d) CPC-photoreactor [41●●]; (e) Annular-system [43]; (f) Stirred tank [38].

lution potential, and its ability of producing strong oxidant species. The fast recombination of photo-generated charge carriers in  $\text{ZnWO}_4$ , was reduced in PEC with the application of a low potential and the combination with graphene oxide [47].

#### 4. Concluding remarks

Photoactive coatings offer a wide range of possibilities to create active surfaces able to inactivate microorganisms. Band gap engineering with the introduction of dopants, or the creation of different junctions allow gaining stability, limit the rate of electron-hole recombination, and can produce materials active under the visible wavelengths of the solar spectrum. Photocatalysis and photoelectrocatalysis offer the possibility of simultaneous removal of pollutants. Besides, photoelectrocatalysis includes the possibility of hydrogen production or other cathodic reactions.

The development of photocatalytic and photoelectrocatalytic surfaces for microbial inactivation must address the following gaps: (1) the development of chemically/photochemically/electrochemically stable and visible light-driven photocatalytic materials for improving sunlight utilization efficiency; (2) the development of nanostructured photoanodes able to provide higher electron transport; (3) the coupling with other processes such as fuel cell or ozonation to improve water disinfection performance; and (4) the design of photocatalytic and photoelectrocatalytic reactors to achieve high efficiency in large-scale applications.

#### Acknowledgements

LV thanks the Spanish Ministry of Education for the FPU grant FPU17/03096.

#### References

1. GKramer A, Schwebke I, Kampf G: How long do nosocomial pathogens persist on inanimate surfaces? A systematic review. *BMC Infect Dis* 2006, 6:130.
2. Kumar A, Alam A, Rani M, Ehtesham NZ, Hasnain SE: Biofilms: Survival and defense strategy for pathogens. *Int J Med Microbiol* 2017, 307:481-489.
3. Wilson AM, Reynolds KA, Sexton JD, Canales RA: Modeling surface disinfection needs to meet microbial risk reduction targets. *Appl Environ Microbiol* 2018, 84:e00709-18.
4. Zhang P, Lin L, Zang D, Guo X, Liu M: Designing bioinspired anti-biofouling surfaces based on a superwettability strategy. *Small* 2017, 13:1503334.
5. Ganguly P, Byrne C, Breen A, Pillai SC: Antimicrobial activity of photocatalysts: Fundamentals, mechanisms, kinetics and recent advances. *Appl Catal B* 2018, 225:51-75.
6. You J, Guo Y, Guo R, Liu X: A review of visible light-active photocatalysts for water disinfection: Features and prospects. *Chem Eng J* 2019, 373:624-641.
7. Singh-Surah S, Vishwakarma M, Kumar R, Nain R, Sirohi S, Kumar G: Tuning the electronic band alignment properties of  $\text{TiO}_2$  nanotubes by boron doping. *Results Phys* 2019, 12:1725-1731.
8. Roy N, Sohn Y, Leung KT, Pradhan D: Engineered electronic states of transition metal doped  $\text{TiO}_2$  nanocrystals for low overpotential oxygen evolution reaction. *J Phys Chem C* 2014, 118:29499-29506.
9. Low J, Yu J, Jaroniec M, Wageh S, Al-Ghamdi AA: Heterojunction photocatalysts. *Adv Mater* 2017, 29:1601694.
10. Ran J, Chen H, Bai X, Bi S, Jiang H, Cai G, Cheng D, Wang X: Immobilizing  $\text{CuO}/\text{BiVO}_4$  nanocomposite on pda-templated cotton fabric for visible light photocatalysis, antimicrobial activity and uv protection. *Appl Surf Sci* 2019, 493:1167-1176.  
• This article reports the use of polydopamine as binder to immobilize  $\text{CuO}/\text{BiVO}_4$ , producing self-cleaning antimicrobial cotton fabrics active under visible light.
11. Wang W, Wang J, Wang Z, Wei X, Liu L, Ren Q, Gao W, Lianga Y, Shia H: p-n junction  $\text{CuO}/\text{BiVO}_4$  heterogeneous nanostructures: synthesis and highly efficient visible-light photocatalytic performance. *Dalton Trans* 2014,43:6735-6743.
12. Yan F, Wang Y, Zhang J, Lin Z, Zheng J, Huang F: Schottky or ohmic metal-semiconductor contact: Influence on photocatalytic efficiency of  $\text{Ag}/\text{ZnO}$  and  $\text{Pt}/\text{ZnO}$  model systems. *ChemSusChem* 2014, 7:101-104.
13. Qiu G, Wang R, Han F, Tao X, Xiao Y, Li B: One-step synthesized  $\text{Au}-\text{Bi}_2\text{WO}_6$  hybrid nanostructures: Synergistic effects of au nanoparticles and oxygen vacancies for promoting selective oxidation under visible light. *Ind Eng Chem Res* 2019, 58:17389-17398.
14. Li B, Tan L, Liu X, Li Z, Cui Z, Liang Y, Zhu S, Yang X, Kwok Yeung KW, Wu S: Superimposed surface plasma resonance effect enhanced the near-infrared photocatalytic activity of  $\text{Au}@\text{Bi}_2\text{WO}_6$  coating for rapid bacterial killing. *J Hazard Mater* 2019, 380:120818.
15. Motola M, Dworniczek E, Satrapinsky L, Chodaczek G, Grzesiak J, Gregor M, Plecenik T, Nowicka J, Plesch G: UV light-induced photo-

- catalytic, antimicrobial, and antibiofilm performance of anodic TiO<sub>2</sub> nanotube layers prepared on titanium mesh and Ti sputtered on silicon. *Chem Pap* 2019, 73:1163-1172. • This work uses magnetron sputtering to create an array of vertically oriented TiO<sub>2</sub> nanotubes on titanium mesh and on silicon substrate.
16. Jalvo B, Faraldos M, Bahamonde A, Rosal R: Antibacterial surfaces prepared by electrospray coating of photocatalytic nanoparticles. *Chem Eng J* 2018, 334:1108-1118.
  17. Jalvo B, Faraldos M, Bahamonde A, Rosal R: Antimicrobial and antibiofilm efficacy of self-cleaning surfaces functionalized by TiO<sub>2</sub> photocatalytic nanoparticles against *Staphylococcus aureus* and *Pseudomonas putida*. *J Hazard Mater* 2017, 340:160-170.
  18. Wang G, Xing Z, Zeng X, Feng C, McCarthy DT, Deletic A, Zhang X: Ultrathin titanium oxide nanosheets film with memory bactericidal activity. *Nanoscale* 2016, 8:18050-18056.
  19. Rtimi S, Pulgarin C, Sanjines R, Nadtochenko V, Lavanchy J-C, Kiwi J: Preparation and mechanism of Cu-decorated TiO<sub>2</sub>-ZrO<sub>2</sub> films showing accelerated bacterial inactivation. *ACS Appl Mater Interfaces* 2015, 7:12832-12839.
  20. Leyland NS, Podporska-Carroll J, Browne J, Hinder SJ, Quilty B, Pillai SC: Highly efficient F, Cu doped TiO<sub>2</sub> anti-bacterial visible light active photocatalytic coatings to combat hospital-acquired infections. *Sci Rep* 2016, 6:24770.
  21. Liu J, Wang Y, Ma J, Peng Y, Wang A: A review on bidirectional analogies between the photocatalysis and antibacterial properties of ZnO. *J Alloys Compd* 2019, 783:898-918.
  22. Valenzuela L, Iglesias A, Faraldos M, Bahamonde A, Rosal R: Antimicrobial surfaces with self-cleaning properties functionalized by photocatalytic ZnO electrosprayed coatings. *J Hazard Mater* 2019, 369:665-673. • This article used electrospray to prepare thin films coatings of ZnO with activity against *Staphylococcus aureus* due to photogenerated ROS and bioavailable Zn<sup>2+</sup>.
  23. Sygellou L, Paterakis G, Galiotis C, Tasis D: Work function tuning of reduced graphene oxide thin films. *J Phys Chem C* 2016, 120:281-290.
  24. Valenzuela L, Iglesias-Juez A, Bachiller-Baeza B, Faraldos M, Bahamonde A, Rosal R: Biocide mechanism of highly efficient and stable antimicrobial surfaces based on zinc oxide-reduced graphene oxide photocatalytic coatings. *J Mater Chem B* 2020, 8:8294-8304.
  25. Wu JM, Kao WT: Heterojunction nanowires of Ag<sub>x</sub>Zn<sub>1-x</sub>O-ZnO photocatalytic and antibacterial activities under visible-light and dark conditions. *J Phys Chem C* 2015, 119:1433-1441.
  26. Ratova M, Redfern J, Verran J, Kelly PJ: Highly efficient photocatalytic bismuth oxide coatings and their antimicrobial properties under visible light irradiation. *Appl Catal B* 2018, 239:223-232.
  27. Fouad M, Gar Alalm M, El-Etriby HK, Boffito DC, Ookawara S, Ohno T, Fujii M: Visible-light-driven photocatalytic disinfection of raw surface waters (300–5000 CFU/mL) using reusable coated Ru/WO<sub>3</sub>/ZrO<sub>2</sub>. *J Hazard Mater* 2021, 402:123514. •• This work uses Ru/WO<sub>3</sub>-ZrO<sub>2</sub> photocatalyst onto aluminium plates for the disinfection of raw wastewater.
  28. Gu Q, Gao Z, Yu S, Xue C: Constructing Ru/TiO<sub>2</sub> heteronanostructures toward enhanced photocatalytic water splitting via a RuO<sub>2</sub>/TiO<sub>2</sub> heterojunction and Ru/TiO<sub>2</sub> Schottky junction. *Adv Mater Interfaces* 2016, 3:1500631.
  29. Wang W, Wang J, Wang Z, Wei X, Liu L, Ren Q, Gao W, Liang Y, Shi H: p-n junction CuO/BiVO<sub>4</sub> heterogeneous nanostructures: Synthesis and highly efficient visible-light photocatalytic performance. *Dalton Trans* 2014, 43:6735-6743.
  30. Ton NQT, Le TNT, Kim S, Dao VA, Yi J, Vu THT: High-efficiency photo-generated charges of ZnO/TiO<sub>2</sub> heterojunction thin films for photocatalytic and antibacterial performance. *J Nanosci Nanotechnol* 2020, 20:2214-2222.
  31. Cho K, Lee S, Kim H, Kim H-E, Son A, Kim E-j, Li M, Qiang Z, Hong SW: Effects of reactive oxidants generation and capacitance on photoelectrochemical water disinfection with self-doped titanium dioxide nanotube arrays. *Appl Catal B* 2019, 257:117910. • This article discusses the effects of capacitance and electrolyte in terms of electrostatic interactions for photoelectrochemical disinfection and degradation of organic compounds.
  32. Pablos C, Marugán J, Adán C, Osuna M, van Grieken R: Performance of TiO<sub>2</sub> photoanodes toward oxidation of methanol and *E. coli* inactivation in water in a scaled-up photoelectrocatalytic reactor. *Electrochim Acta* 2017, 258:599-606.
  33. Ding M, Shi F, Zhu H, Yang Y, Zhong J, Luo L, Huo Y, Li H: Photoelectrocatalytic bacterial inactivation of *acinetobacter baumannii* on Cu<sub>2</sub>O/TiO<sub>2</sub>@Cu mesh photoanodes. *Catal Sci Technol* 2020, 10:7378-7385.
  34. Jiang Q, Yin H, Li G, Liu H, An T, Wong PK, Zhao H: Elimination of antibiotic-resistance bacterium and its associated/dissociative *bla*TEM-1 and *aac*(3)-II antibiotic-resistance genes in aqueous system via photoelectrocatalytic process. *Water Res* 2017, 125:219-226.

35. Juodkazytė J, Petrulevičienė M, Parvin M, Šebeka B, Savickaja I, Pakštas V, Naujokaitis A, Virkutis J, Gegeckas A: Activity of sol-gel derived nanocrystalline WO<sub>3</sub> films in photoelectrochemical generation of reactive chlorine species. *J Electroanal Chem* 2020, 871:114277.
36. Salmerón I, Sharma PK, Polo-López MI, Tolosana A, McMichael S, Oller I, Byrne JA, Fernández-Ibáñez P: Electrochemically assisted photocatalysis for the simultaneous degradation of organic micro-contaminants and inactivation of microorganisms in water. *Process Saf Environ* 2021, 147:488-496. • This paper points out the key role of the cathode material in photoelectrocatalytic disinfection and presents an improvement using a carbon-based cathode for the selective reduction of molecular oxygen to hydrogen peroxide.
37. Souza BA, Perini JA, Giannini MJSM, Zanoni MVB: Fast removal of candida parapsilosis from hemodialysis dialysate using ultraviolet or visible light at nanoporous W/WO<sub>3</sub> electrodes. *J Environ Chem Eng* 2019, 7:103104.
38. Zhan S, Zhou F, Huang N, He Q, Zhu Y: Deactivating harmful marine microorganisms through photoelectrocatalysis by GO/ZnWO<sub>4</sub> electrodes. *Chem Eng J* 2017, 330:635-643.
39. Zhang G, Zhang Z, Xia D, Qu Y, Wang W: Solar driven self-sustainable photoelectrochemical bacteria inactivation in scale-up reactor utilizing large-scale fabricable Ti/MoS<sub>2</sub>/MoO<sub>x</sub> photoanode. *J Hazard Mater* 2020, 392:122292.
40. Zheng Z, He J, Dong C, Lo IMC: Photoelectrochemical sewage treatment by sulfite activation over an optimized BiVO<sub>4</sub> photoanode to simultaneously promote PPCPs degradation, H<sub>2</sub> evolution and *E. coli* disinfection. *Chem Eng J* 2021, 419:129418. •• This paper used the visible light activation of sulphite to promote disinfection and pollutant degradation on the anode and hydrogen production on the cathode.
41. McMichael S, Waso M, Reyneke B, Khan W, Byrne JA, Fernandez-Ibanez P: Electrochemically assisted photocatalysis for the disinfection of rainwater under solar irradiation. *Appl Catal B* 2021, 281:119485. •• This article presents the design of a concentric tubular photoelectrocatalytic reactor with a CPC for solar bacterial inactivation using rainwater as electrolyte.
42. Giannakis S, Polo López, MI, Spuhler, D, Sánchez-Pérez, JA, Fernández-Ibáñez, P, Pulgarin, C: Solar disinfection is an augmentable, in situ-generated photo Fenton reaction—Part 1: A review of the mechanisms and the fundamental aspects of the process. *Appl Catal B Environ* 2016, 199:199-223.
43. Kim JYU, Bessegato GG, de Souza BC, da Silva JJ, Zanoni MVB: Efficient treatment of swimming pool water by photoelectrocatalytic ozonation: Inactivation of *Candida parapsilosis* and mineralization of benzophenone-3 and urea. *Chem Eng J* 2019, 378:122094.
44. Mesones S, Mena E, López-Muñoz MJ, Adán C, Marugán J: Synergistic and antagonistic effects in the photoelectrocatalytic disinfection of water with TiO<sub>2</sub> supported on activated carbon as a bipolar electrode in a novel 3D photoelectrochemical reactor. *Separ Purif Technol* 2020, 247:117002.
45. Domínguez-Espíndola RB, Bruguera-Casamada C, Silva-Martínez S, Araujo RM, Brillas E, Sirés I: Photoelectrocatalytic inactivation of *Pseudomonas aeruginosa* using an Ag-decorated TiO<sub>2</sub> photoanode. *Separ Purif Technol* 2019, 208:83-91.
46. He H, Sun S, Gao J, Huang B, Zhao T, Deng H, Wang X, Pan X: Photoelectrocatalytic simultaneous removal of 17 $\alpha$ -ethinylestradiol and *E. coli* using the anode of Ag and SnO<sub>2</sub>-Sb 3D-loaded TiO<sub>2</sub> nanotube arrays. *J Hazard Mater* 2020, 398:122805.
47. Zhan S, Zhou F, Huang N, Liu Y, He Q, Tian Y, Yang Y, Ye F: Synthesis of ZnWO<sub>4</sub> electrode with tailored facets: Deactivating the microorganisms through photoelectrocatalytic methods. *Appl Surf Sci* 2017, 391:609-616.
48. Valenzuela L, Faraldos M, Bahamonde A, Rosal R: High performance of electrosprayed graphene oxide/TiO<sub>2</sub>/Ce-TiO<sub>2</sub> photoanodes for photoelectrocatalytic inactivation of *S. aureus*. *Electrochim. Acta* 2021, 395:139203.
49. Wu S, Hu YH: A comprehensive review on catalysts for electrocatalytic and photoelectrocatalytic degradation of antibiotics. *Chem Eng J* 2021, 409:127739.
50. Moreira FC, Boaventura RAR, Brillas E, Vilar VJP: Electrochemical advanced oxidation processes: A review on their application to synthetic and real wastewaters. *Appl Catal B* 2017, 202:217-261.